

## MODELLING OF WAVES AND WAVE-STRUCTURE INTERACTIONS USING NON-LINEAR NUMERICAL MODELS

AXELLE VIRÉ\*, JOHANNES SPINNEKEN†, MATTHEW D. PIGGOTT‡,  
CHRISTOPHER C. PAIN‡ AND STEPHAN C. KRAMER‡

\*Delft University of Technology  
Faculty of Aerospace Engineering  
Kluyverweg 1, 2629 HS Delft, The Netherlands  
e-mail: a.c.vire@tudelft.nl

†Imperial College London  
Department of Civil and Environmental Engineering  
South Kensington Campus, SW7 2AZ London, United Kingdom

‡Imperial College London  
Department Earth Science and Engineering  
South Kensington Campus, SW7 2AZ London, United Kingdom

**Key words:** Fluid-structure interactions, Immersed-body method, Wave modelling, Unstructured finite-element methods, Offshore piles

**Abstract.** The aim of this study is to validate a fully non-linear finite-element model to simulate waves and wave-structure interactions. The Navier–Stokes equations are solved on an extended domain, which covers both fluid and structure. The latter is represented by a non-zero solid-concentration field, which is computed by conservatively mapping a mesh discretising the solid onto the extended mesh. In the regions of non-zero solid concentration, a penalty force is further added to the equations of motion in order to represent the effect of the structure on the fluid dynamics. The results are first shown for the interactions between a cylindrical pile and a regular train of small-amplitude gravity waves in a numerical wave tank. The pile is considered both as an immersed body and as a void in the fluid domain. In both cases, good overall agreement is obtained between the numerical and theoretical predictions of the free-surface elevation. The immersed-body approach however tends to underestimate the water elevation in the vicinity of the structure, due to additional dissipation induced by the body force. Second, the generation of focused wave events is considered. Preliminary results suggests that the present model is capable of modelling focused wave events propagating in the numerical wave tank. This is a first step towards modelling the interactions between pile and steep irregular waves.

## 1 INTRODUCTION

The accurate computation of wave loads is important in offshore engineering, for example, to optimally design oil and gas platforms or coastal defense structures. In recent years, there has also been an increased interest in offshore renewable-energy devices, which can be either mounted on the sea bed (fixed devices) or moored to it (floating devices). In this context, an accurate prediction of the wave loading is vital to ensure that offshore renewable-energy devices are economically viable and can withstand rough sea conditions. Numerical models can assist in the design of these devices by analysing several different configurations, while limiting expensive laboratory or onsite testing. The hydrodynamic behaviour is however complex due to: (i) the interactions between extreme waves and solid structures (for fixed and floating devices), and (ii) the mutual interactions between fluids and moving solids (for floating devices). The proposed method aims at tackling both aspects, although only fixed solids are considered in this study.

The modelling techniques for wave-structure interactions are reviewed in the literature [1], in the context of wave energy converter arrays. The methods differ depending on whether the flow is potential or not. If the flow is potential and the structure is a bottom-mounted cylinder, the scattering of plane waves in the linear diffraction regime is described by a Laplace equation for the velocity potential and a set of boundary conditions. This problem has an analytical solution [2]. It is also commonly solved numerically using the so-called boundary element method, which works on either a linearised formulation of the problem (linear potential models) or the non-linear formulation (non-linear potential models). Although linear approaches operate in the frequency domain and are not computationally demanding, they are restricted to constant fluid depths. By contrast, non-linear approaches work in the time domain and include important terms in the free surface boundary conditions (and body forcing) which can be very significant. They can also model transient phenomena and account for nonlinear external forces, despite the potential flow assumption. Therefore, non-linear potential models are extensively used for computing extreme loads on fixed and moving structures. For example, a fully nonlinear potential method was used to calculate the wave radiation due to prescribed oscillations of a submerged sphere [3]. Wu and Eatock Taylor [4] performed a similar analysis with an oscillating cylinder in two dimensions and showed that, in this context, the boundary element method was more efficient computationally than a finite-element method. Non-linear wave interactions with three-dimensional fixed and floating vertical cylinders are extensively analysed using potential-flow models, including high-order methods [5, 6, 7, 8].

When the flow is not potential, computational fluid dynamics (CFD) models provide a tool to account for viscous and rotational effects on the flow by numerically solving the Navier-Stokes equations. Thus, CFD models can compute extreme wave loading, for which viscous effects and air entrainment cannot be neglected. However, the accurate

prediction of wave propagation using CFD models is difficult. In [9], it was shown that most CFD models currently available fail to accurately model waves propagating over long distances. This is due to the inherent energy dissipation introduced by the discretisation schemes used for the Navier-Stokes equations. A high-order free-surface method was recently implemented in the CFD model Fluidity [10, 11] and showed very promising results on the simulation of linear gravity waves in a numerical wave tank [15].

The purpose of this study is twofold. First, it aims at validating the immersed-body method in the context of wave-structure interactions. Second, it extends our previous work to the simulation of focused wave events of increasing steepness propagating in a numerical wave tank. The paper is organised as follows. Section 2 describes the mathematical formulation of the immersed-body method and the fluid-dynamics model. Results are detailed in Section 3 for two cases: (i) wave-structure interactions for a cylindrical pile subjected to a regular train of waves, and (ii) focused wave events propagating in a numerical wave tank. Finally, conclusions are drawn in Section 4.

## 2 MATHEMATICAL FORMULATION AND METHODOLOGY

This study uses the computational fluid dynamics model Fluidity [10, 11] to numerically solve the Navier–Stokes equations. Two approaches are compared to model waves interacting with solid structures. On the one hand, the Navier–Stokes equations are solved on a mesh surrounding the solid structures (defined-body method). This technique can give accurate results, when using appropriate discretisation schemes and sufficient spatial resolution, because the solid shape and boundary conditions are represented exactly. However, if the solid moves in the fluid domain, re-meshing is necessary. This is computationally expensive and might yield highly-distorted grids. The immersed-body method [12, 13] was developed to avoid this problem. It consists in filling the regions covered by the structure with the surrounding fluid, and relaxing the flow to the structure’s behaviour in those regions. The flow problem is thus solved for a monolithic velocity  $\mathbf{u} = \hat{\mathbf{u}}_f + \hat{\mathbf{u}}_s$ , where  $\hat{\mathbf{u}}_f = \alpha_f \mathbf{u}_f$ ,  $\hat{\mathbf{u}}_s = \alpha_s \mathbf{u}_s$ , and  $(\alpha_f, \alpha_s)$  are the fluid- and solid- concentration fields such that  $\alpha_f + \alpha_s = 1$  throughout the domain. Assuming that the fluid is incompressible, the continuity equation for the monolithic velocity is expressed as

$$\nabla \cdot \mathbf{u} = 0. \tag{1}$$

The variation of fluid momentum on the extended mesh is given by

$$\rho \frac{\partial \mathbf{u}}{\partial t} + \rho (\mathbf{u} \cdot \nabla) \mathbf{u} = -\nabla p + \nabla \cdot (2\mu \overline{\overline{\mathbf{S}}}) + \mathbf{F}_f + \mathbf{B}, \tag{2}$$

where  $\rho$  is the fluid density,  $p$  is the pressure field,  $\mu$  is the dynamic viscosity of the fluid,  $\overline{\overline{\mathbf{S}}}$  is the deviatoric part of the strain-rate tensor  $S_{ij} = \partial_j u_i + \partial_i u_j$ . The relaxation of the flow velocity to the solid velocity is achieved through the volumetric penalty force

$\mathbf{F}_f$ , so that the no-slip boundary condition is not explicitly imposed along the fluid-solid interface. The force is zero except close to the fluid-solid interface, and is expressed as

$$\mathbf{F}_f = \beta (\hat{\mathbf{u}}_s - \alpha_s \mathbf{u}), \quad (3)$$

where  $\beta = \max\left(\frac{\rho}{\Delta t} + \frac{\mu}{L^2}\right)$  ( $\Delta t$  being the time step and  $L$  the local edge length) is a relaxation factor which dictates how fast the fluid and solid velocities equal each other at the interface [12]. The magnitude of the relaxation factor is driven by viscous effects at small Reynolds numbers and inertial effects at large Reynolds numbers.

The solid-concentration field  $\alpha_s$  is needed to enforce the penalty condition (Eq. 3), and also to locate the structure on the extended computational mesh. The computation of  $\alpha_s$  is performed as follows:

1. Loop over the elements  $E_s$  of the structural mesh.
2. For each element of  $E_s$ :
  - Construct the super-mesh  $\mathcal{S}$  [14] by identifying the elements of the extended mesh  $E_f$  that intersect  $E_s$ .
  - Project a unitary field (which is the value of  $\alpha_s$  on the structural mesh) from structural- to super- mesh using a Galerkin projection. This yields  $\alpha_s^{\mathcal{S}}$ .
3. Project  $\alpha_s^{\mathcal{S}}$  from super- to fluid- mesh using a Galerkin projection.

Details about the discretisation method, including the conservative Galerkin projection via a super-mesh, are described in [12]. In this work, time is discretised using a Crank–Nicolson scheme.

### 3 RESULTS

#### 3.1 Regular waves

The ability to simulate regular waves in the absence of a pile using Fluidity is demonstrated in [15]. This study applies the immersed-body approach to the numerical simulation of regular waves interacting with a fixed pile. Figure 1 shows a sketch of the domain, which has a total length of  $51D$ , a width of  $34D$  and a depth of  $2.4D$  ( $D$  being the pile diameter). The centre of the cylindrical pile is placed at a distance of  $34D$  from the tank outlet, and  $17D$  from the inlet and sides. The horizontal, lateral and vertical directions are denoted by  $x$ ,  $y$ , and  $z$  respectively.

The flow is considered as inviscid, in order to enable direct comparison with existing analytical theories. Regular waves propagating are generated by setting the horizontal

velocity at the inlet ( $x = 0$ ) to the linear wave kinematics solution. Linear waves of constant steepness  $ak = 0.001$  are considered, where the wave amplitude is defined as  $a = H/2$  and  $H = a_{\text{crest}} + a_{\text{trough}}$ . The wavenumber  $k$  is further related to the wave frequency  $\omega = 2\pi T$  by the following dispersion equation

$$\omega^2 = gk \tanh(kh), \quad (4)$$

where  $g$  is the acceleration due to gravity and  $h$  is the water depth. In this study,  $kh = 2.84$ . Defining the deep-water wave-length as  $\lambda_0 = 2\pi g/\omega^2$ , the present non-dimensional water depth is further equal to  $h/\lambda_0 = 0.45$ . At the outlet of the domain, the velocity components are left free and the non-hydrostatic part of the pressure field is naturally set to zero. An absorption layer is also used in the region  $34D \leq x \leq 51D$  to avoid spurious wave reflections. To this end, the artificial absorption term  $\sigma u$  is added to the right-hand-side of the fluid momentum equation, where

$$\sigma = \begin{cases} \frac{1}{4} \left( \tanh \left[ \frac{\sin(\pi(4\tilde{x}-1)/2)}{1-(4\tilde{x}-1)^2} \right] + 1 \right) & \text{if } 0 \leq \tilde{x} \leq \frac{1}{2} \\ \frac{1}{4} \left( \tanh \left[ \frac{\sin(\pi(3-4\tilde{x})/2)}{1-(3-4\tilde{x})^2} \right] + 1 \right) & \text{if } \frac{1}{2} \leq \tilde{x} \leq 1, \end{cases} \quad (5)$$

with  $\tilde{x} = (x - L_0)/L$  and  $L = 17D$  is the length of the absorption layer [16]. A normal flow condition is used at the bottom and lateral sides of the tank, while a combined pressure and free-surface kinematic boundary condition is prescribed for the top surface [17, 18]. The domain is discretised using a mixed finite-element discretisation method, where discontinuous linear polynomials are used for the velocity field (i.e. P1-DG discretisation) and continuous piecewise quadratic polynomials are used for the pressure field (i.e. P2 discretisation). Two different approaches for representing the pile are compared. In the defined-body case, the fluid mesh excludes the region occupied by the pile. The pile contour is meshed in the  $x$ - $y$  plane by 32 mesh elements, whose typical edge length is  $l_e = D/10$ . The mesh size increases to  $l_e = D/2$  at the sides of the domain. Representing the solid as a hole in the fluid domain is the classical approach for modelling fluid flow around a fixed solid structure. By contrast, in the immersed-body approach, the fluid mesh covers the entire wave tank and a separate solid mesh discretises the three-dimensional pile. The position of the solid within the fluid mesh is represented through a solid-concentration field, which is computed following the procedure explained in Section 2. In this study, both approaches use an unstructured mesh in the  $x$ - $y$  plane, which is extruded vertically into tetrahedra using fourteen uniformly-spaced layers. The two-dimensional mesh in the  $x$ - $y$  plane is composed of 15,000 nodes in the defined-body case and 10,000 nodes in the immersed-body case. In the latter, the three-dimensional pile is further discretised by an unstructured mesh composed of 1,000 nodes.

Figure 2 shows the evolution of the free-surface elevation in the horizontal direction, at the pile centreline and  $t = 20T$  ( $T$  being the wave period). The continuous line shows the theoretical solution based on [2]. Symbols represent the numerical result for the

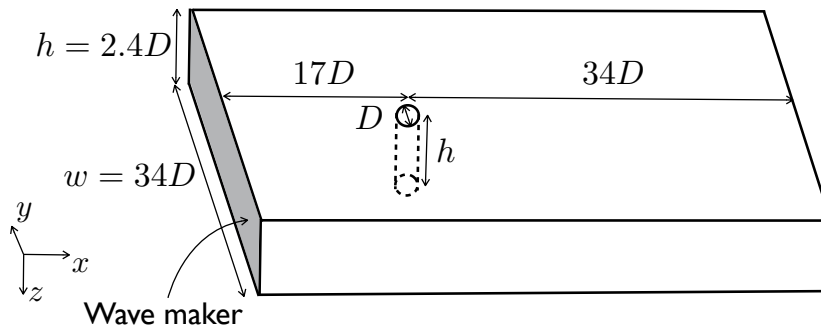


**Figure 1:** Sketch of the numerical wave tank.

defined-body case, while the dashed line shows the immersed-body results. The grey area further illustrates the location of the pile. Good overall agreement is observed between the numerical and theoretical predictions of the free-surface elevation. However, local discrepancies are observed in the immersed-body results. In particular, the free-surface elevation is under-estimated in the vicinity of the pile. There are mainly two possible explanations for this behaviour. First, this could be due to a lack of spatial resolution close to the pile, since the spatial resolution around the pile is coarser in the immersed-body case than in the defined-body simulation. Second, the penalty force given by Eq. 3 induces an additional absorption term in the Navier–Stokes equations that can affect the wave amplitude in the vicinity of the pile. Ongoing work is focussing on analysing the effect of mesh refinement on the accuracy of the numerical results, for a wider range of wave conditions.

### 3.2 Focused waves

In practice, most waves are irregular. This section tackles the simulation of irregular waves using Fluidity. The computational domain is identical to the numerical wave tank considered in the previous section, except that the wave maker generates a steep transient wave groups and the pile is removed. The focused wave events are such that the maximum wave amplitude occurs at a distance  $x_f = 10h$  from the input boundary and a time of  $t_f = 16T$  ( $T$  being the wave period of the previous section). Three values are considered for the sum of focused event amplitude:  $A_{\text{sum}}k_p = 100.54; 502.65; 1005.3$  ( $k_p$  being the wave number corresponding to the peak in JONSWAP spectrum). Since it is numerically challenging to have a stable solution for large values of the wave steepness when the flow is inviscid, a uniform kinematic viscosity of  $\nu = 10^{-3} \text{ m}^2\text{s}^{-1}$  is used in the present simulations as viscous damping. Ongoing work is currently investigating a numerical stabilisation method to add minimal dissipation attempting to minimise the effect on the accuracy of the method.

Figures 3 to 5 show the time evolution of the free-surface elevation at  $x_f = 10h$  for three

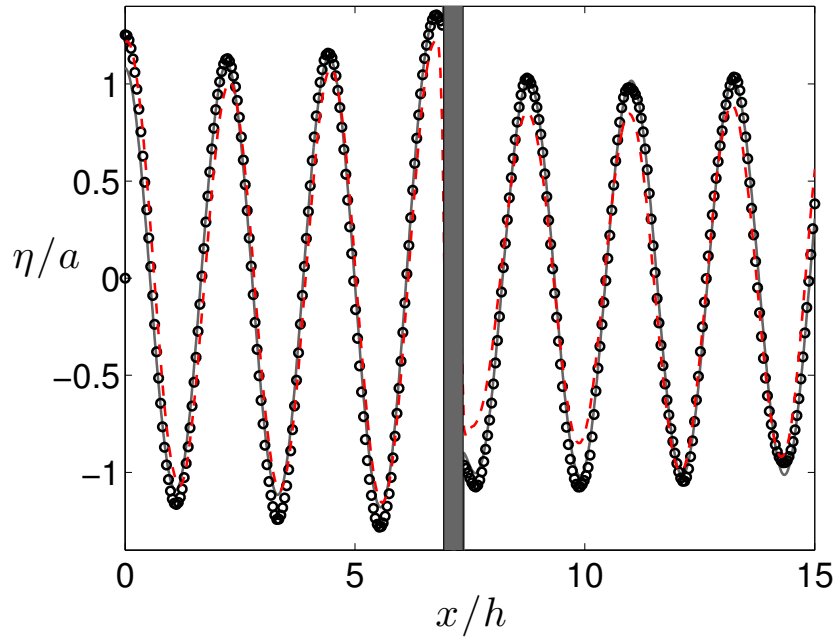


**Figure 2:** Non-dimensionalised surface elevation  $\eta/a$  at  $t = 20T$  for  $ak = 0.001$  and  $h/\lambda_0 = 0.45$ . The continuous line is the wave amplitude calculated using linear diffraction theory. The symbols represent the numerical results for the defined-body case, while the dashed line shows the immersed-body results. The grey area represents the location of the pile.

values of the focused event amplitude:  $A_{\text{sum}}k_p = 100.54$  (Fig. 3),  $A_{\text{sum}}k_p = 502.65$  (Fig. 4), and  $A_{\text{sum}}k_p = 1005.3$  (Fig. 5). The continuous line represents second-order theoretical calculation [19], while symbols show the present numerical results. It is apparent in the three plots that the event focusses at  $t = 16T$ . Figure 3 shows that the numerical result of the surface elevation agrees well with the theoretical calculation at  $A_{\text{sum}}k_p = 100.54$ . At higher values of  $A_{\text{sum}}k_p$ , a departure from the second-order calculation is expected due to the presence of higher-order components. The present numerical results predict well this departure, for example, through a downstream shift of the focused location, see Figs. 4-5. Although these results look promising, further analysis is ongoing to assess the effect of resolution and viscous damping on the results.

## 4 CONCLUSIONS

This work combines a high-order free-surface method with a fluid-structure interaction algorithm to simulate waves and wave-structure interactions in a numerical wave tank. Preliminary results show that the proposed methodology is capable of simulating: (i) regular and irregular waves propagating in a numerical wave tank, and (ii) wave-structure interactions with a fixed structure. For the latter, good overall agreement is shown between the defined- and immersed- body approaches, when a bottom-mounted pile is placed in the numerical wave tank. The immersed-body approach however underestimates the

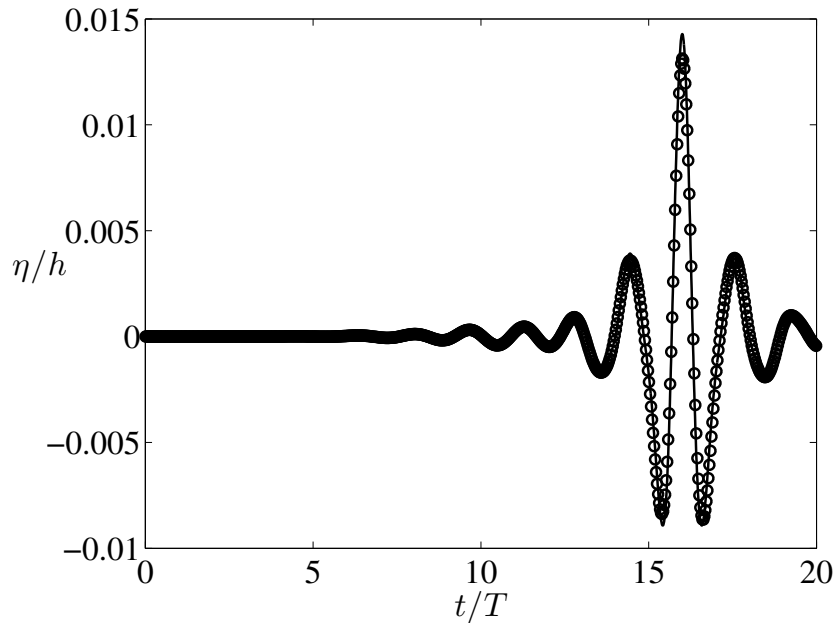


**Figure 3:** Surface elevation  $\eta(t)$  for a focused event of amplitude  $A_{\text{sum}}k_p = 100.54$  at  $x_f = 24D$ . The continuous line represents second-order calculation, while symbols are the present numerical results.

water elevation in the vicinity of the structure. Two possible explanations for this effect are: (i) lack of spatial resolution around the pile, and/or (ii) additional dissipation induced by the immersed-body force. Future work will focus on: (i) the effect of increased spatial resolution on the accuracy of the numerical results, (ii) the effect of turbulence models on the propagation of focused wave events, and (iii) a wider range of linear and nonlinear wave conditions. This work is a first-step towards the fully non-linear simulation of steep irregular waves interacting with a structure.

## ACKNOWLEDGMENTS

A. Viré is supported by the European Union Seventh Framework Programme (FP7/2007-2013) under a Marie Curie Career Integration Grant (grant agreement PCIG13-GA-2013-618159). She also acknowledges support from Imperial College London and its High Performance Computing Service, as well as Université Libre de Bruxelles. The content of this paper reflects only the authors views and not those of the European Commission.

## REFERENCES

- [1] Folley, M., Babarit, A., Child, B., Forehand, D., O’Boyle, L., Silverthorne, K., Spinneken, J., Stratigaki, V. and Troch, P. A review of numerical modelling of wave energy converter arrays, *Proc. of the ASME 31st International Conference on Ocean, Offshore and Arctic Engineering* (2012) 7:535–546.

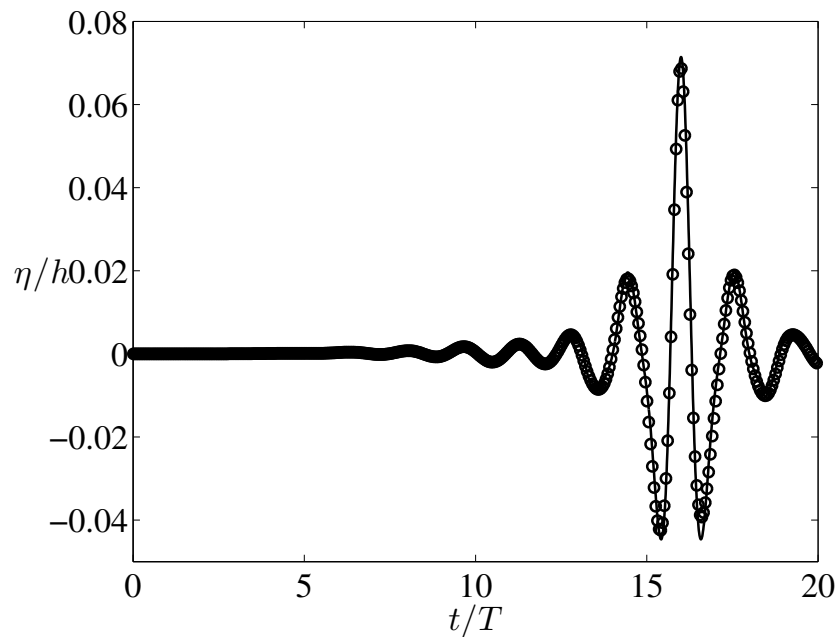


**Figure 4:** Surface elevation  $\eta(t)$  for a focused event of amplitude  $A_{\text{sum}}k_p = 502.65$  at  $x_f = 24D$ . The continuous line represents second-order calculation, while symbols are the present numerical results.

- [2] MacCamy, R.C. and Fuchs, R.A. Wave forces on piles: a diffraction theory, Technical Memorandum, *U.S. Beach Erosion Board* (1954) **69**.
- [3] Lee, C.C., Liu, Y.H. and Kim, C.H.. Simulation of nonlinear wave and forces due to transient and steady motion of submerged sphere, *Int. J. Offshore Polar Eng.* (1994) **4**:174–182.
- [4] Wu, G.X. and Eatock Taylor, R. Time stepping solutions of the two-dimensional nonlinear wave radiation problem, *Ocean Eng.* (1995) **22**:785–798.
- [5] Hu, P.X., Wu, G.X. and Ma, Q.W. Numerical simulation of nonlinear wave radiation by a moving vertical cylinder. *Ocean Eng.* (2002) **29**:1733–1750.
- [6] Bai, W. and Eatock Taylor, R. Higher-order boundary element simulation of fully nonlinear wave radiation by oscillating vertical cylinders. *Appl. Ocean Res* (2006) **28**:247–265.
- [7] Bai, W. and Eatock Taylor, R. Fully nonlinear simulation of wave interaction with fixed and floating flared structures, *Ocean Eng.* (2009) **36**:223–236.
- [8] Ma, Q.W. and Patel, M.H. On the non-linear forces acting on a floating spar platform in ocean waves, *Appl. Ocean Res.* (2001) **23**:29–40.

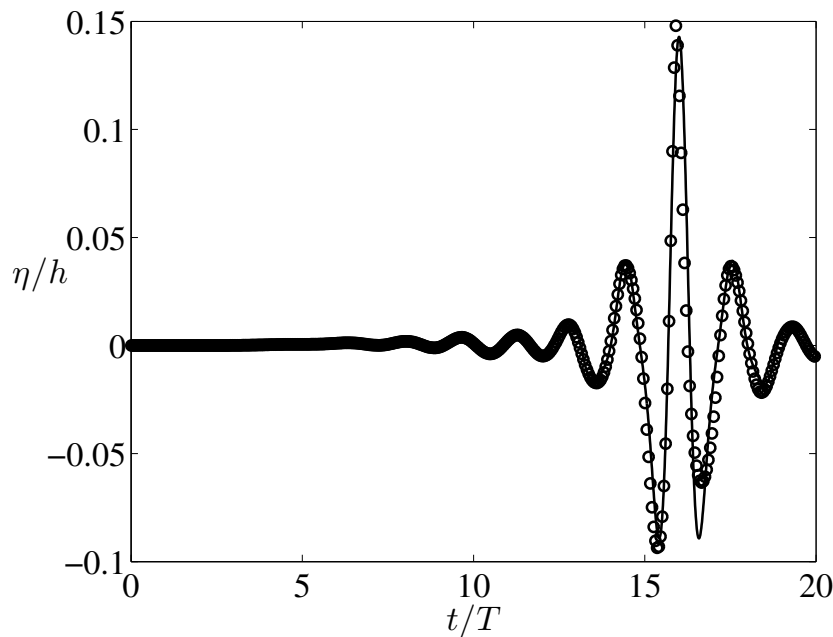


**Figure 5:** Surface elevation  $\eta(t)$  for a focused event of amplitude  $A_{\text{sum}k_p} = 1005.3$  at  $x_f = 24D$ . The continuous line represents second-order calculation, while symbols are the present numerical results.

- [9] Maguire, A.E. Geometric design considerations and control methodologies for absorbing wavemakers, *PhD Thesis*, The University of Edinburgh (2011).
- [10] Pain, C.C., Piggott, M.D., Goddard, A.J.H., Fang, F., Gorman, G.J., Marshall, D.P., Eaton, M.D., Power, P.W. and de Oliveira, C.R.E. Three-dimensional unstructured mesh ocean modelling. *Ocean Model.* (2005) **10**:5–33.
- [11] Piggott, M.D., Farrell, P.E., Wilson, C.R., Gorman, G.J. and Pain, C.C. Anisotropic mesh adaptivity for multi-scale ocean modelling, *Phil. Trans. R. Soc. A* (2009) **367**:4591–4611.
- [12] Viré, A., Xiang, J., Milthaler, F., Farrell, P., Piggott, M.D., Latham, J.-P., Pavlidis, D. and Pain, C.C. Modelling of fluid-solid interactions using an adaptive mesh fluid model coupled with a combined finite-discrete element model, *Ocean Dyn.* (2012) **62**:1487–1501.
- [13] Viré, A. How to float a wind turbine. *Rev. Environ. Sci. Biotechnol.* (2012) **11**:223–226.
- [14] Farrell, P.E., Piggott, M.D., Pain, C.C., Gorman, G.J. and Wilson, C.R. Conservative interpolation between unstructured meshes via supermesh construction, *Comput. Methods Appl. Mech. Eng.* (2009) **198**:2632–2642.

- [15] Viré, A., Xiang, J., Piggott, M.D., Spinneken, J. and Pain, C.C. Numerical modelling of fluid-structure interactions for floating wind turbines foundations, *Proc. of the 23rd International Ocean and Polar Engineering Conference, Alaska* (2013).
- [16] Stelling, G. and Zijlema, M. An accurate and efficient finite-difference algorithm for non-hydrostatic free-surface flow with application to wave propagation, *Int J Numer Meth Fluids* (2003) **43**:1–23.
- [17] Funke, S.W., Pain, C.C., Kramer, S.C. and Piggott, M.D., A wetting and drying algorithm with a combined pressure/free-surface formulation for non-hydrostatic models, *Advances in Water Resources* (2011) **34**:1483–1495.
- [18] Oishi, Y., Piggott, M.D., Maeda, T., Kramer, S.C., Collins, G.S., Tsushima, H. and Furumura, T., Three-dimensional tsunami propagation simulations using an unstructured mesh finite element model, *Journal of Geophysical Research: Solid Earth* (2013) **118**:2998–3018.
- [19] Sharma, J.N. and Dean, R.G. Second-order directional seas and associated wave forces. *Society of Petroleum Engineers Journal* (1981) **21**:129–140.